Mon. Not. R. Astron. Soc. **000**, 1–?? (2014) Printed 15 July 2014 (MN LATEX style file v2.2)

The hunt for red AGN: a new infrared diagnostic

Dario Fadda[(1)⋆], Giulia Rodighiero[(2)]

[(1)] *IPAC, Caltech 100-22, CA 91125 Pasadena*
[(2)] *Dipartimento di Fisica e Astronomia, Università di Padova, vicolo dell'Osservatorio 3, I–35122 Padova, Italy.*

ABSTRACT

We introduce a new infrared diagnostic to separate galaxies on the basis of their dominant infrared emission: stellar or nuclear. The main novelty with respect to existing diagnostics, is the usage of a broad band encompassing at the same time the 9.7μm Silicate absorption feature and one of the adjacent broad PAH (polycyclic aromatic hydrocarbon) features. This provides a robust estimate of the near- to mid-infrared continuum slope and enables a clear distinction among different classes of galaxies up to a redshift $z \sim 2.5$. The diagnostic can be applied to a wealth of archival data from the ISO, Spitzer, and Akari surveys as well as future JWST surveys. Based on data in the GOODS, Lockman Hole, and North Ecliptic Pole (NEP) fields, we find out that approximately 70% active galactic nuclei detected with X-ray and optical spectroscopy dominate the total mid-infrared emission. Finally, we estimate that AGN contribute less than 30% of the mid-infrared extragalactic integrated emission.

Key words: cosmology: observations – galaxies: active – galaxies: evolution – galaxies: starburst – infrared: galaxies.

1 INTRODUCTION

Star forming regions and active galactic nuclei (AGN) are often embedded in dust which reprocesses high-energy radiation to infrared emission. Infrared surveys are therefore the ideal way to detect this kind of systems. The most active star-forming regions are embedded in dust and contribute most of the extra-galactic integrated infrared emission (see, e.g. Fadda et al. 2002, Pozzi et al. 2012). On the other hand, obscured AGN can be detected in the infrared but it is sometimes difficult to separate them from star-forming dominated systems (Feltre et al. 2012, Delvecchio et al. 2014). The same obscured AGN are responsible for the unresolved part of the hard X-ray cosmic background (e.g. Gilli et al. 2007). Even deep X-ray surveys are unable to resolve a substantial part of the background in the hard X-ray regime. When more than 90% of the soft X-ray background has been resolved with recent Chandra and XMM surveys (Tozzi et al. 2006, Hasinger et al. 2001), only 50% of the sources in the hard X-ray band 5-10 keV are currently resolved (Worsley et al. 2005, Shi et al. 2013).

Waiting for new X-ray detectors in the ultra-hard energy regime (∼30 keV) which will be able to directly see the unobscured AGN, we can exploit existing icnfrared surveys to uncover this population of highly extinguished AGN. With the advent of *Spitzer*, several new techniques have been suggested to select AGN in infrared surveys. Some of them make use of near- and mid-infrared colours (Lacy et al. 2004, Stern et al. 2005, Daddi et al. 2007, Hanami et al. 2012, Donley et al. 2012, Messias et al. 2012, Stern et al. 2012, Juneau et al. 2013, see Caputi et al. 2014 for a review). More recently, *Herschel* far-infrared fluxes have been combined with other wavelengths to constrain the obscured AGN content in dusty galaxies, through colours and SED fitting decomposition (e.g. Berta et al. 2013, Kirkpatrick et al. 2013). However, *Herschel* surveys are not as deep as mid-infrared *Spitzer* surveys. Despite their success, these techniques suffer of a high degree of contamination especially at high redshifts and fail to detect Seyfert type-2 galaxies. We propose here a new infrared diagnostic which makes use of a broad mid-infrared band obtained by combining two filters from the *Spitzer*, *ISO* and *Akari* surveys. The computed colours are not affected by the highly variable spectral features in the mid-infrared wavelength range, allowing a clear distinction among different classes of galaxies in a large redshift range ($0 < z < 2.5$).

We apply the diagnostic to *Spitzer* observations in the GOODS field, *ISO* and *Spitzer* observations in the Lockman Hole, and *Akari* in the NEP field. Results are compared with X-ray detections and optical spectroscopy of AGN in the fields. An estimate of the AGN contribution to the mid-infrared cosmic background is presented. Throughout this paper we use $H_0 = 70$ km s^{-1} Mpc^{-1}, $\Omega_m = 0.3$, $\Omega_\Lambda = 0.7$.

⋆ E-mail: fadda@ipac.caltech.edu

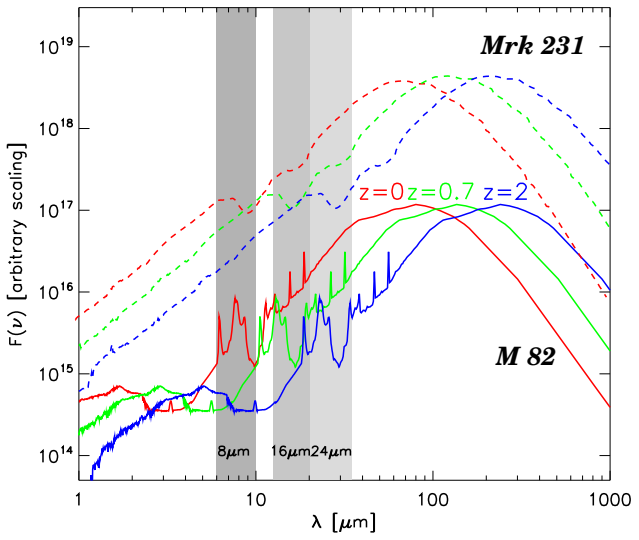

Figure 1. The 8, 16, and 24 μm filter coverage of SEDs of a star forming galaxy (M82, solid lines) and an AGN dominated one (Mrk231, dashed lines) at 3 different redshifts.

2 A NEW INFRARED DIAGNOSTIC

Several infrared diagnostics have been proposed to distinguish AGN from star forming galaxies. These diagnostics are able to separate statistically most of the AGN at low redshifts ($z < 1$) while they become severely contaminated at higher redshifts. Moreover, tracks of type 2 Seyfert degenerate on the plots with starburst galaxies (Rodighiero et al. 2007). Some otherstudies (see, e.g., Martínez-Sansigre et al. 2005, Daddi et al. 2007, Fiore et al. 2008, Fadda et al. 2010, Kirkpatrick et al. 2012) use also 24μm fluxes to select AGN candidates and confirm them through spectroscopy and/or comparison with X-ray images.

Using the mid-infrared 24μm flux is, in principle, a very powerful method to find obscured AGN. The main problem comes from the fact that the mid-infrared region is full of broad spectral features: two bands of PAH (polycyclic aromatic hydrocarbon) and the 9.7μm Silicate absorption. The extreme variability of these features among star forming galaxies and AGN (see Spoon et al. 2007) makes extremely difficult to use the 24μm in combination with fluxes at other wavelengths (e.g. the 8μm IRAC) as a diagnostic. As shown by Brand et al. (2006), the 24μm/8μm colour cannot be used in a large range of redshifts to distinguish AGN and star-forming objects. To overcome these problems, we propose here to use the $(S_{24}+S_{16})/S_{8.0}$ colour. As shown in Figure 2, this flux ratio is much less disturbed by the broad mid-infrared spectral features in a large redshift range ($0 < z < 2.5$). In fact, when one of the filters falls into the Silicate absorption the other one is on the top of a PAH feature, compensating for the missing flux. The combination of the two filters gives therefore a more stable estimate of the continuum and the proposed flux ratio is, in the redshift interval between 0 and 2.5, a good estimate of the near- to mid-infrared spectral slope. Combining this flux ratio with the IRAC $S_{5.8}/S_{3.6}$ colour, we obtain a very clean diagnostic.

Figure 2 shows the tracks of a set of templates (see caption for references) in the range $0.1 < z < 2.5$ spanning four main classes: ellipticals, spirals, AGN and starburst galaxies. The four classes are well separated in this plot, thus proving the strength of this diagnostic to classify infrared selected galaxies. Note, in particular, that the Seyfert 2 template (Sy2, in the AGN region) is not degenerate with other star-forming galaxies (like late spirals), as instead usually happens for other infrared diagnostics (e.g. Lacy et al. 2005). Rare objects like the extremely absorbed F00183-711 contaminates the starburst region only at high redshifts ($z > 2$). The diagnostic becomes less efficient at redshifts larger than 2.5 when the 1.6μm stellar bump enters the 8μm filter affecting the continuum slope estimate. By using the template library of Dale et al. (2014), we verified that objects with emission dominated by AGN (AGN emission greater than 50% of the total emission) are selected by our diagnostic.

The same idea can be applied with different sets of filters from other infrared telescopes, as *ISO* and *Akari*. In the case of *ISO*, the LW3 band (centered around 15μm) can be used instead of the IRS16. For *Akari* (see Figure 2), one can use the broad L18W band or the sum of the L24+L15 bands. Also a combination of *Akari* and *Spitzer* bands can be used as displayed in Figure 2. This is especially useful, since the three telescopes have publicly accessible archives.

Furthermore, future surveys with the MIRI instrument on board the James Webb Space Telescope will also provide a set of filters[1] suited to apply the proposed diagnostic.

3 DATA

In order to apply the proposed diagnostic, we used a set of publicly available *Spitzer*, *ISO*, and *Akari* data in four different deep fields: GOODS North, GOODS South, Lockman Hole, and North Ecliptic Pole (NEP). The first three fields have been observed with Legacy (SWIRE, Londsale et al. 2003) and GTO programs with *Spitzer* in all the infrared bands of IRAC and MIPS. IRAC and MIPS highly processed images are available from the *Spitzer* archive. *ISO* observations of the Lockman Hole with ISOCAM in the LW3 band have been published by the authors (Fadda et al. 2004, Rodighiero et al. 2004). Moreover, the two GOODS fields have been observed with IRS onboard *Spitzer* at 16μm. These data are now publicly available from the *Spitzer* archive and we have retrieved and processed them.

To reduce the 16μm data we started from the basic calibrated data (BCD) available from the *Spitzer* archive. Stacking all the BCDs, we obtained a superflat which has been applied to the single BCDs. Since we are only interested in the point sources in the field, we subtracted also the median background from each BCD before mosaicking them in a single image. We used the *Spitzer* software MOPEX to obtain a mosaic with a pixel half the size of the original ones using the redundancy of the observations to reject outliers.

For the source extraction we used a PSF fitting method (Starfinder, Diolaiti et al. 2000) for the 16μm and MIPS 24μm data and aperture photometry with SExtractor (Bertin & Arnout, 1996) for the IRAC images. In the case of IRAC images, in fact, PSF fitting techniques are hampered by the undersampling of the PSF. A critical step to apply the

[1] In particular, to achieve a broad-band as large the 16μm+24μm *Spitzer* filter, one could combine the three MIRI filters F1500W, F1800W and F2550W.

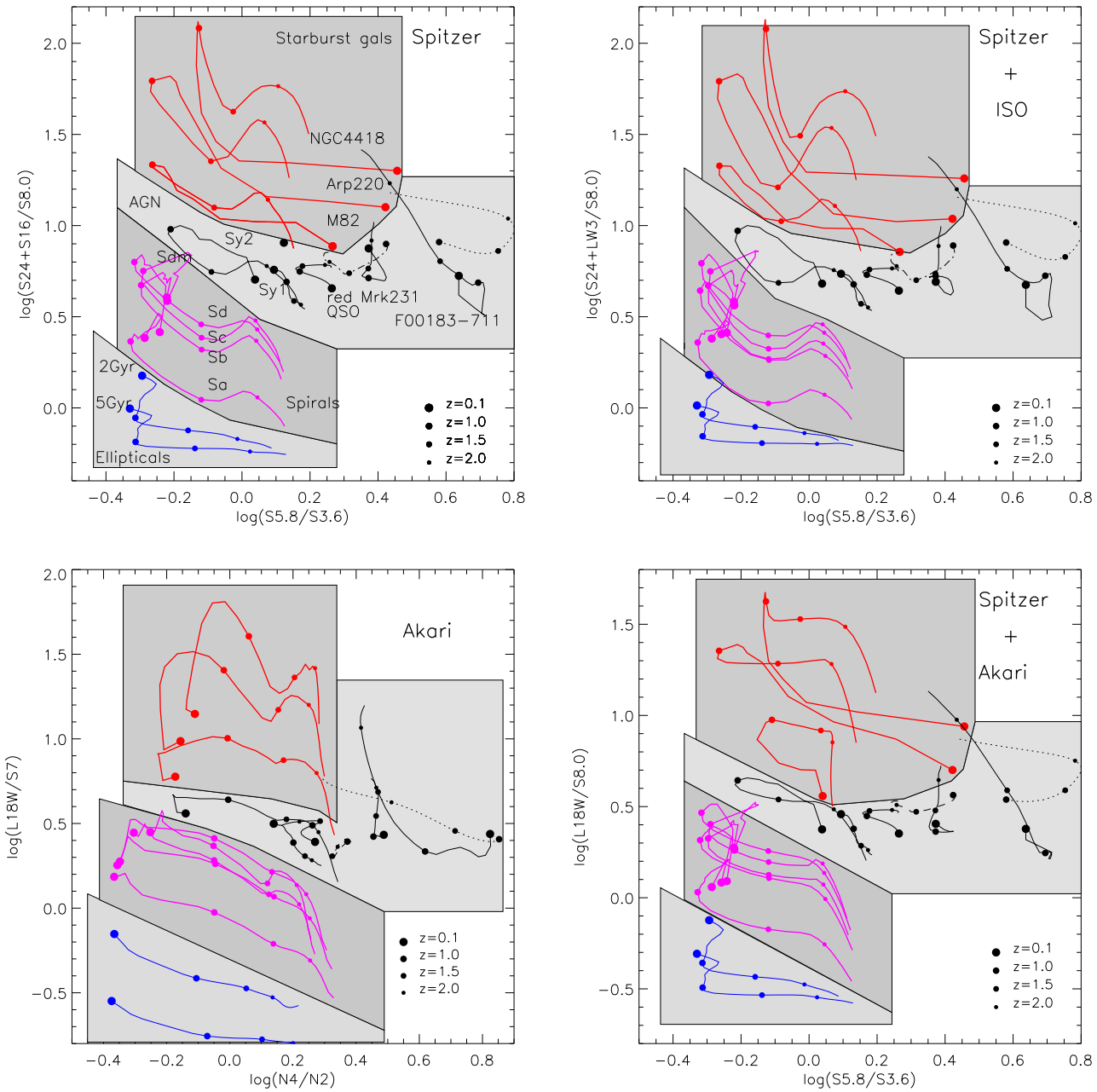

Figure 2. The new infrared diagnostic proposed for four different combination of filters of *ISO*, *Spitzer* and *Akari*. Tracks in the redshift range $0.1 < z < 2.5$ are of templates from Polletta et al. (2007, M82, Sa, Sb, Sc, Sd, Arp220, Sy1, Red QSO, Ell 2Gyr, Ell 5Gyr), Spoon et al. (2007, NGC4448 and F00183-7111) and Gruppioni et al. (2010, Sy2, Mrk231, and Sdm). Templates of $z > 1$ high-τ AGN (Sajina et al. 2012) and Silicate AGN (Kirkpatrick et al. 2012) are marked with black dotted and dot-dashed lines, respectively. We define four regions occupied by different classes of infrared sources.

colour diagnostic proposed in the paper is to accurately compute aperture corrections for the different filters. As shown by Fadda et al. (2006), the 24μm theoretical PSF obtained using STinyTim[2] accurately reproduces the real 24μm PSF. The same is true for the 16μm array. So, in these cases, we fitted a PSF inside the aperture of 9.45 arcsec and 14.0 arcsec radii for the 16μm and 24μm bands, respectively. The aperture correction computed was of 1.1626 and 1.158 for the 16μm and 24μm bands, respectively.

In the case of IRAC, the real PSF is significantly different from that produced with STinyTim and the model cannot be used to compute aperture corrections. So, we used the values computed with a set of stars in the SWIRE fields (see

[2] irsa.ipac.caltech.edu/data/SPITZER/docs/dataanalysistools/tools/contributed/general/stinytim

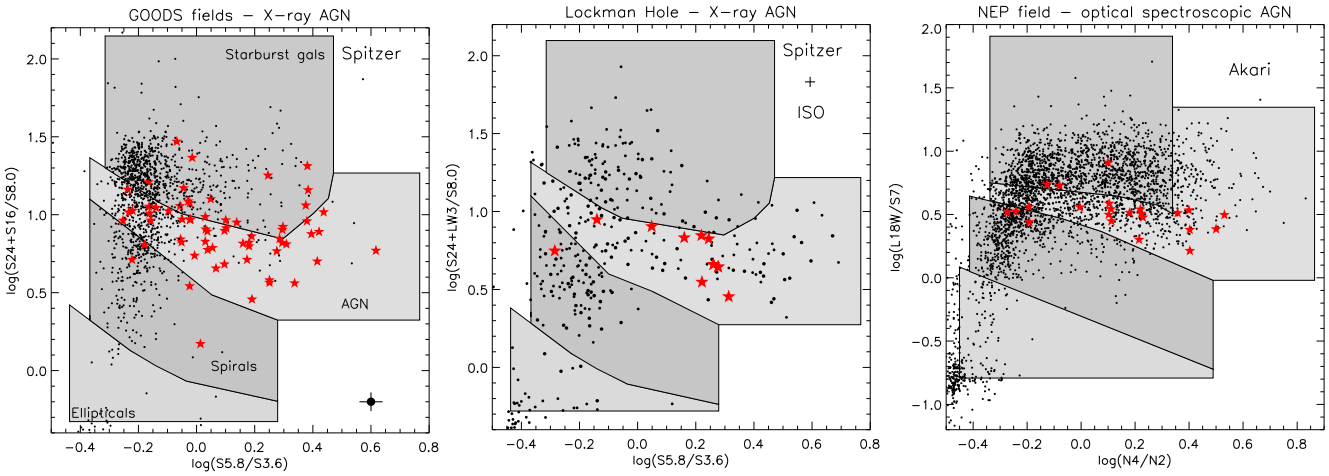

Figure 3. Diagnostic applied to 3 deep fields with AGN shown as red stars: *Left:* GOODS and X-ray sources with $L_{2-8keV} > 10^{42.5} L_{\odot}$ (Alexander et al., 2003); *Middle:* Lockman Hole and X-ray sources with $L_{2-10keV} > 10^{42.5} L_{\odot}$; *Right:* NEP field (Murata et al., 2013) and sources spectroscopically classified as AGN by Shim et al. (2013). The typical photometric error, assuming 10% and 5% errors in mid-IR and near-IR fluxes, respectively, is reported in the right-bottom corner.

SWIRE data release report[3], page 31). Using 3.8 arcsec diameter apertures, we applied corrections of 1.35, 1.39, 1.65, and 1.84 for the 3.6, 4.5, 5.8, and 8.0 μm IRAC channels, respectively.

The final catalogs have been matched starting from the 16μm (or 15μm) catalog using a matching radius of 2 arcsec. The 16μm and 24μm filters are expected to be sensitive to different redshift regions because the 9.7μm Si absorption affects them at different redshifts. In our cases, because of the depth of the IRAC and MIPS images, only a few 16μm sources do not have MIPS counterparts. Above 0.1 mJy, the percentage of 16μm sources without MIPS counterparts is negligible (less than 10%) for all the surveys here considered. For fluxes fainter than 0.1 mJy, the percentage is slightly higher: in particular, for GOODS-North the percentage is still around 10% down to 0.06mJy, while for the UDF the percentage gets worse in the fainter flux bin considered in the following discussion (30-40% in the range 0.04-0.06 mJy).

For what concerns the NEP *Akari* field, we rely completely on published photometry (Murata et al. 2013).

4 COMPARISON WITH X-RAY AND SPECTROSCOPIC SELECTIONS

X-ray surveys are one of the cleanest methods to select AGN since they probe directly their high energy emission. However, the situation is more complex when dusty tori obscure the X-ray emission and reprocess it into infrared emission. For these reasons, the AGN detections through X-ray and infrared are somewhat complementary. However, when using infrared bands to detect AGN, we have to remember that dusty tori are not usually the main contributors to the total infrared emission except for the very bright end of the infrared population (see, i.e., Brand et al. 2006).

To test how many of the infrared sources classified as AGN based on their X-ray emission are classified as AGN by the our diagnostic, we considered three fields which have been observed with *Spitzer* and *ISO* in the infrared and with *Chandra* (Alexander et al. 2003) and *XMM* (Hasinger et al. 2001) in the X-ray. We can apply the diagnostic using only *Spitzer* data to the two GOODS fields which have been observed with IRAC and MIPS with the GOODS legacy survey. To compute the X-ray luminosities, we used a compilation of redshifts for the GOODS fields[4] and redshifts from Lehmann et al. (2001) for the Lockman Hole. As shown in Figures 3, most of the sources with high X-ray fluxes (i.e. $L_{2-10keV} > 10^{42.5} L_{\odot}$), that are probably AGN, fall in the AGN locus of our empirical diagnostic. Taking into account photometric errors, (70 ± 10)% of the GOODS X-ray sources fall in the AGN locus. The percentage is approximately 90% in the case of the Lockman Hole. As already pointed out, the diagnostic is not expected to be 100% accurate because of the mixed source of infrared emission in galaxies. Especially for distant AGN, the host galaxy can produce enough stars to mask the AGN behaviour in the low resolution *Spitzer* images. On the contrary, in the case of X-ray observations, the AGN dominates the total emission even in the case of low resolution images.

In the NEP field, where a complete *Akari* photometric catalog is available (Murata et al. 2013), we can test our diagnostic against a selection of AGN sources classified on the basis of their optical emission lines (Shim et al. 2013). 70^{+10}_{-5}% of the optically detected AGN are classified as infrared sources with emission dominated by the AGN by our diagnostic.

Our findings are compatible with the study of Polletta et al. (2007) who find that ~ 80% of X-ray selected AGN are identified as AGN using their infrared SEDs when the redshift of the source is known, and with Donley et al. (2012) who were able to recover 75% of the X-ray sources brighter than $L_{2-10keV} = 10^{44} erg/s$ with their IRAC color selection technique. On the basis of these comparisons, we argue that

[3] swire.ipac.caltech.edu/swire/astronomers/publications/SWIRE2_doc_083105.pdf

[4] www.eso.org/sci/activities/garching/projects/goods/MasterSpectroscopy

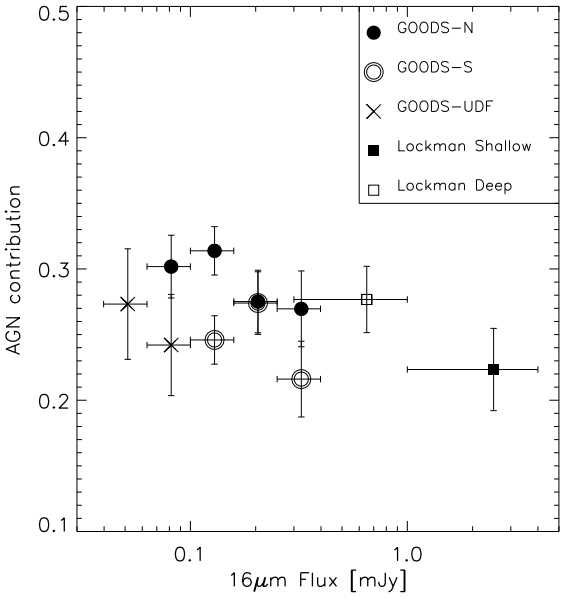

Figure 4. AGN contribution to the cosmic infrared background at 16μm as a function of the flux using surveys in three different fields.

the proposed diagnostic can be safely used to obtain an estimate of the AGN contribution to the mid-IR background. A further validation of the diagnostic with SED fitting decomposition (including a dusty torus component) is deferred to a forthcoming paper (Baronchelli et al., in preparation).

5 AGN CONTRIBUTION TO THE MID-IR BACKGROUND

To compute the AGN contribution to the mid-IR background, we considered the sum of the fluxes of the sources falling in the AGN loci defined in Figure 2. The total extragalactic flux has been computed by adding the fluxes of all the sources which are not stars. In our diagnostic, stars fall at the bottom of the colour diagram and can be easily rejected. Figure 4 reports the fraction of AGN flux from the different fields in several flux bins. Poissonian error bars are reported. Due to the low number of sources, errors are still rather large but all the measurements are consistent and give an estimate of the AGN contribution between 20% and 30%. The fraction is larger than the estimate done in the Lockman Hole using only X-ray identified AGN by Fadda et al. (2002) and is closer to more recent estimates based on *Spitzer* 24μm data (Choi et al. 2011). A better coverage of the mid-infrared region with future JWST surveys will allow the selection of large samples of highly obscured AGN.

ACKNOWLEDGMENTS

We thank the referee for his/her suggestions that improved the clarity of the paper. GR acknowledges support from the University of Padova from ASI (Herschel Science Contract I/005/07/0). This work is based in part on observations made with *Spitzer*, a space telescope operated by the Jet Propulsion Laboratory, California Institute of Technology under a contract with NASA. Support for this work was provided by NASA through an award issued by JPL/Caltech. We thank Alberto Franceschini for useful comments.

REFERENCES

Alexander, D. M., et al. 2003, AJ, 126, 539
Berta, S., Lutz, D., Santini, P., et al. 2013, A&A, 551, A100
Bertin, E., & Arnouts, S. 1996, A&AS, 117, 393
Brand, K., et al. 2006, ApJ, 644, 143
Caputi, K. I. 2014, arXiv:1405.7940
Choi, P. I., Yan, L., Helou, G., et al. 2011, ApJ, 732, 21
Daddi, E., et al. 2007, ApJ, 670, 173
Dale, D. A., et al. 2014, ApJ, 784, 83
Delvecchio, I., et al. 2014, MNRAS, 439, 2736
Diolaiti, E., et al. 2000, A&AS, 147, 335
Donley, J. L., et al. 2012, ApJ, 748, 142
Fadda, D. et al. 2002, A&A, 383, 838
Fadda, D. et al. 2004, A&A, 427, 23
Fadda, D., et al. 2006, AJ, 131, 2859
Fadda, D., Yan, L., Lagache, G., et al. 2010, ApJ, 719, 425
Fiore, F., Grazian, A., Santini, P., et al. 2008, ApJ, 672, 94
Gilli, R., Comastri, A., & Hasinger, G. 2007, A&A, 463, 79
Gruppioni, C., et al. 2010, A&A, 518, L27
Hanami, H., et al. 2012, PASJ, 64, 70
Hasinger, et al. 2001, A&A, 365, L45
Juneau, S., et al. 2013, ApJ, 764, 176
Kirkpatrick, A., et al. 2012, ApJ, 759, 139
Kirkpatrick, A., et al. 2013, ApJ, 763, 123
Lacy et al. 2004
Lehmann, I., et al. 2001, A&A, 371, 833
Lonsdale, C.J. et al., 2003, PASP, 115, 897
Martínez-Sansigre, A., et al. 2005, Nature, 436, 666
Messias, H., et al. 2012, ApJ, 754, 120
Murata, K., et al. 2013, A&A, 559, A132
Polletta, M., et al. 2007, ApJ, 663, 81
Pozzi, F., et al. 2012, MNRAS, 423, 1909
Rodighiero, G. et al. 2004, A&A, 427, 773
Rodighiero, G. et a.l 2007, MNRAS, 376, 416
Sajina, A., et al. 2012, ApJ, 757, 13
Shi, Y., et al. 2013, ApJ, 764, 28
Shim, H., Im, M., Ko, J., et al. 2013, ApJS, 207, 37
Spoon, H. W. W., et al. 2007, ApJL, 654, L49
Stern, D., et al. 2005, ApJ, 631, 163
Stern, D., et al. 2012, ApJ, 753, 30
Tozzi, P., Gilli, R., Mainieri, V., et al. 2006, A&A, 451, 457
Worsley, M. A., Fabian, A. C., Bauer, F. E., et al. 2005, MNRAS, 357, 1281